Sleep Spindle Detection Using Time-Frequency Sparsity

Ankit Parekh*, Ivan W. Selesnick*, David M. Rapoport†, Indu Ayappa†
* Dept. of Electrical and Computer Engineering, NYU School of Engineering, Brooklyn, NY.
† Dept. of Medicine, Division of Pulmonary, Critical Care and Sleep Medicine, NYU School of Medicine, New York, NY.

***Abstract*— This paper proposes an EEG processor for sleep spindle detection algorithms. It non-linearly separates the raw EEG signal into non-oscillatory transient and sustained rhythmic oscillation components using long and short windows for the short-time Fourier transform. The processor utilizes the fact that sleep spindles can be sparsely represented via the inverse of a short-time Fourier transform. Five sleep spindle detectors were tested on the EEG database with and without the proposed EEG processor. We achieved an improvement of 13.3% in the by-sample F_1 score, and 13.9% in the by-sample Matthews Correlation Coefficient score of these algorithms when the processed EEG was used for spindle detection. The processor was able to improve the scores by reducing the number of false positive spindles and increasing the number of true positive spindles detected.**

***Index Terms*—Short time Fourier transform, spectrogram, convex optimization, pursuit algorithms**

I. Introduction

Sleep spindles comprise of a group of rhythmic waves that progressively increase and decrease in amplitude [32]. They are measured by electroencephalography (EEG) and the duration of these waves range from 0.5 to 3 seconds [37]. Any spindle-like waveform that has a duration less than 0.5 seconds is generally not considered a sleep spindle [25], [32]. The frequency range of spindles is between 12 and 14 Hz [25]. However, recent studies have extended this range to 11-16 Hz [35], [24], [9], [8].

It is believed that sleep spindles play an important functional role in synaptic plasticity and memory consolidation during sleep [13]. Alterations in their density have been observed in EEG of several patients with disorders such as schizophrenia [12], [34], autism [18], other neurodegenerative and sleep disorders [23]. For this reason, it is thought that sleep spindles may be valuable as diagnostic biomarkers [35].

Traditionally, spindles have been identified and scored visually by experts in sleep clinics. The experts have been trained to not only detect spindles, but also classify the patient's EEG data into different stages of sleep. The patient's EEG is divided into 30 second epochs and scored [32]. This is a labor intensive and subjective method of detecting spindles. Further complicating the detection process is the low inter-expert agreement of spindle identification [38].

A. State-of-the-art

Several detectors have been developed in the past few decades with their number growing in the past few years. Most of the widely used detectors employ the method of bandpass filtering and amplitude thresholding [26], [12], [34], [36], [4], [14], [20]. Several spindle detectors employ advanced methods such as artificial intelligence [16], [17], neural networks [15], likelihood [22] and support vector machines [1]. Some of the detection algorithms are able to extract and classify features other than sleep spindles [21].

Time-frequency analysis using the short-time Fourier transform (STFT) is a commonly used method for spindle detection [7], [15], [6]. The peaks in the spectrogram obtained using the STFT can be used to detect sleep spindles. Another adaptive time-frequency method of signal analysis is Matching Pursuit (MP) [19]. The idea of MP was used in sleep spindle detection as early as 1996 [11] and more recently in [16], [17]. The performance of MP, however, for sleep spindle detection of healthy male subjects was not at par with the other detectors employing more basic detection methods [27].

 This work was supported by the NSF under Grant No. CCF-1018020.

B. Motivation

The EEG is a non-stationary signal exhibiting a mixture of oscillatory and non-oscillatory transient behaviors. It possesses rhythmic oscillations as well as transients due to measurement artifacts and non-rhythmic brain activity. Furthermore, the bandpass filter used by the sleep spindle detection algorithms is excited by these transients in the EEG. As a result, the spindle activity in the bandpass filtered data is not always prominent. This emphasizes the need for the separation of the sustained oscillations and the non-oscillatory transients. Separation of these components for analysis using linear methods is difficult. On the other hand, non-linear methods have the potential to process and analyze complex non-stationary signals more efficiently than linear methods [29].

In this paper, we present a non-linear method that separates the transients from the sustained rhythmic oscillations and apply it to the problem of sleep spindle detection. This non-linear method acts as a processor for algorithms that use bandpass filtering as a means to detect spindles. Using the proposed processor, the algorithms in [34], [36], [4], [14], and [20] see significant improvement in sleep spindle detection.

II. Preliminaries

A. Notation

Vectors and matrices are represented by lower- and upper-case bold letters respectively. For a vector $\mathbf{x} = [x_0, \ldots, x_{N-1}], \mathbf{x} \in \mathbb{R}^N$, the l_1 and l_2 norms are defined as

$$||\mathbf{x}||_1 = \sum_{k=1}^{N} |x_k|, \qquad ||\mathbf{x}||_2 = \left(\sum_{k=1}^{N} |x_k|^2 \right)^{1/2} \tag{1}$$

Further, the root mean square (RMS) value of the vector $\mathbf{x}$ is defined as

$$\mathbf{x}_{\text{rms}} = \left(\frac{1}{N} \sum_{k=1}^{N} |x_k|^2 \right)^{1/2} \tag{2}$$

B. Basis Pursuit Denoising

Utilizing convex optimization, basis pursuit denoising (BPD) finds signal representations in over-complete transforms by minimizing the l_1 norm of the representation coefficients [5]. Minimizing the l_1 norm results in a sparse representation for the signal $\mathbf{x}$. Sparse representations are representations which account for most of the information in a signal with a linear combination of a small number of representation coefficients. If we define the input signal $\mathbf{y}, \in \mathbb{R}^N$ as

$$\mathbf{y} = \mathbf{A}\mathbf{c} + \mathbf{w} \tag{3}$$

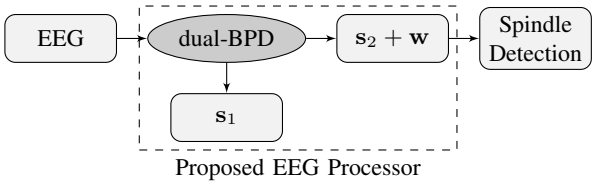

Fig. 1. The proposed dual-BPD EEG processor. The processor decomposes the input EEG channel into two components $\mathbf{s}_1, \mathbf{s}_2$ and the residual $\mathbf{w}$. The long-window component along with the residual $(\mathbf{s}_2 + \mathbf{w})$ is used for spindle detection.

where the columns of $\mathbf{A}$ form an over-complete basis for $\mathbb{R}^N$, and $\mathbf{w}$ is the residual, then basis-pursuit denoising (BPD) yields an approximation to $\mathbf{y}$ by minimizing the following objective function-

$$\arg\min_{\mathbf{c}} \frac{1}{2}||\mathbf{y} - \mathbf{A}\mathbf{c}||_2^2 + \lambda||\mathbf{c}||_1 \tag{4}$$

BPD admits the presence of a residual in the decomposition which is useful for practical signals that contain measurement artifacts. A similar type of sparse approximation method is matching pursuit (MP). MP, compared to BPD, has a tendency of selecting coefficients wrongly, thereby resulting in an erroneous approximation, in the initial iterations [5]. This forces the MP algorithm to make alternating corrections suggesting a complex structure for the input signal. Due to this, the original structure of the input signal is often missed entirely [5].

C. Short-time Fourier Transform

For the sparse representation of an input signal consisting of oscillatory pulses, $\mathbf{A}$ in (3) can be taken as the inverse of a short-time Fourier transform (STFT). The STFT depends on the window length, overlapping factor and the discrete Fourier transform (DFT) length. We use 93.75% overlapping between the windows, i.e., a hop-size of 1/16 of the window length and a DFT length equal to the window length. Consequently, the STFT is 16 times over-sampled. Moreover, if the time-frequency array of the STFT coefficients $\mathbf{c}$ is of size $M \times K$, for a signal $\mathbf{y}$ of length N, then $\mathbf{A} : \mathbb{C}^{M\times K} \rightarrow \mathbb{C}^N$ is defined as

$$[\mathbf{A}\mathbf{c}]_n = \left[\text{STFT}^{-1}(\mathbf{c})\right]_n, \qquad n \in \mathbb{Z}_N \tag{5}$$

whereas $\mathbf{A}^H : \mathbb{C}^N \rightarrow \mathbb{C}^{M\times K}$ is defined as

$$[\mathbf{A}^H\mathbf{y}]_{(m,k)} = [\text{STFT}(\mathbf{y})]_{(m,k)}, \qquad m \in \mathbb{Z}_M, k \in \mathbb{Z}_K \tag{6}$$

We implement $\mathbf{A}$ using a sine window such that $\mathbf{A}\mathbf{A}^H = \mathbf{I}$ as in [28].

III. Dual Basis Pursuit Denoising

We model the raw EEG signal as

$$\mathbf{y} = \mathbf{s}_1 + \mathbf{s}_2 + \mathbf{w}, \qquad \mathbf{y}, \mathbf{s}_1, \mathbf{s}_2, \mathbf{w} \in \mathbb{R}^N \tag{7}$$

where $\mathbf{s}_1, \mathbf{s}_2$ are vectors which are sparsely represented using the over-complete transforms $\mathbf{A}_1, \mathbf{A}_2$, and $\mathbf{w}$ is the residual obtained after the decomposition. This kind of a model is used in 'Morphological Component Analysis' (MCA) for non-linear separation of signal components [33].

For the separation of the non-oscillatory transients and the sustained oscillations, we use $\mathbf{A}_1$ and $\mathbf{A}_2$ to be the inverse STFT using different window lengths. We use a short window for $\mathbf{A}_1$ to sparsely represent the transients and a long window for $\mathbf{A}_2$ for representing the sustained rhythmic oscillations.

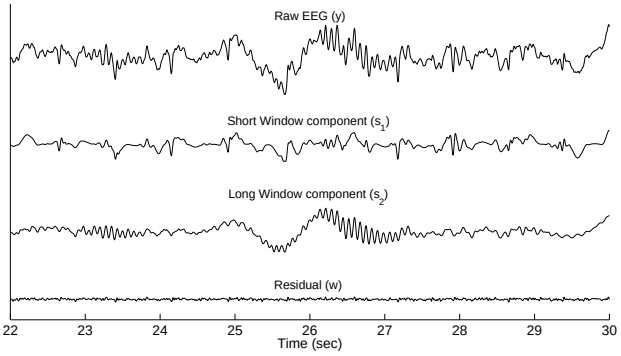

Fig. 2. The raw EEG decomposed into the short $(\mathbf{s}_1)$ and long window $(\mathbf{s}_2)$ components using dual-BPD. The residual $\mathbf{w}$ obtained after the decomposition is also shown.

Given $\mathbf{y}$ we will estimate $\mathbf{s}_1, \mathbf{s}_2$ by solving the following minimization problem-

$$\{\mathbf{c}_1^*, \mathbf{c}_2^*\} = \arg\min_{\mathbf{c}_1,\mathbf{c}_2} \frac{1}{2}||\mathbf{y} - \mathbf{A}\mathbf{c}_1 - \mathbf{A}\mathbf{c}_2||_2^2 + \lambda_1||\mathbf{c}_1||_1 + \lambda_2||\mathbf{c}_2||_1 \tag{8}$$

The individual components $\mathbf{s}_1, \mathbf{s}_2$ are then estimated as

$$\mathbf{s}_i = \mathbf{A}_i\mathbf{c}_i^* \qquad i = 1, 2. \tag{9}$$

If we let

$$\mathbf{A} = [\mathbf{A}_1 \quad \mathbf{A}_2], \quad \mathbf{c} = [\mathbf{c}_1 \quad \mathbf{c}_2]^T \tag{10}$$

where

$$\mathbf{A}_i\mathbf{A}_i^H = \mathbf{I}, \quad i = 1, 2 \tag{11}$$

then using the split augmented Lagrangian shrinkage algorithm (SALSA) as in [2], [30], and [31] we obtain the following algorithm for solving (8)

Algorithm 1 dual-BPD (8) with $\mathbf{A}_i\mathbf{A}_i^H = \mathbf{I}$

inputs:

$\mathbf{y} \in \mathbb{R}^N, \lambda_1, \lambda_2, \mu$

initialize:

$\mathbf{d}_i, \mathbf{c}_i \in \mathbb{C}^{M\times K}$

repeat

$\mathbf{v}_i \leftarrow \text{soft}\left(\mathbf{c}_i + \mathbf{d}_i, \lambda_i/\mu\right) - \mathbf{d}_i, \quad i = 1, 2$

$\mathbf{d}_i \leftarrow \frac{1}{\mu+2}\mathbf{A}_i^H\left[\mathbf{y} - \mathbf{A}_1\mathbf{v}_1 - \mathbf{A}_2\mathbf{v}_2\right], \quad i = 1, 2$

$\mathbf{c}_i \leftarrow \mathbf{d}_i + \mathbf{v}_i, \quad i = 1, 2$

until convergence

return $\mathbf{c}_1, \mathbf{c}_2$

The soft-threshold function, soft$(\mathbf{x}, T)$ is defined as in [10], generalized here to the complex plane.

Figure 2 shows the decomposition of the raw EEG using dual-BPD. The sum of the three components shown, $\mathbf{s}_1$, $\mathbf{s}_2$ and $\mathbf{w}$ equals the raw EEG, emphasizing that none of the information in the raw EEG is lost. Further, it can be seen that $\mathbf{s}_1$ contains the non-oscillatory transients and none of the sustained oscillations in the input signal $\mathbf{y}$. The sustained oscillations are contained in $\mathbf{s}_2$ component.

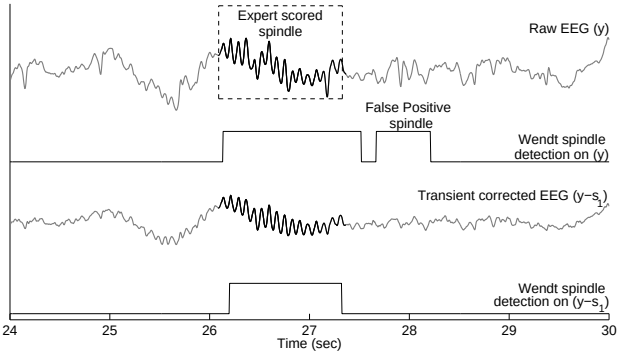

Fig. 3. A false positive spindle detected by the Wendt algorithm applied on the raw EEG. The false positive is not produced by the Wendt algorithm when the transient corrected EEG, instead of the raw EEG, is used for spindle detection.

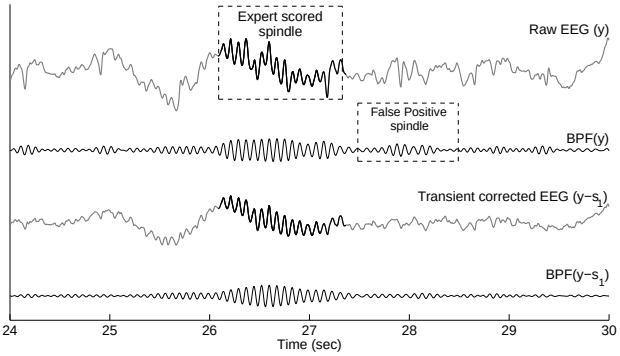

Fig. 4. The raw and processed EEG filtered with the bandpass filter (BPF) used by the Wendt algorithm for spindle detection.

IV. Examples

To illustrate sleep spindle detection using the dual-BPD processor, we apply dual-BPD to the C3-A1 channel of the EEG. The algorithms in [36] and [20] are then used to detect spindles. The database used in this and the following example is explained in Section V-A.

We use a window length of 0.32 seconds for $\mathbf{A}_1$ and a window length of 1.28 seconds for $\mathbf{A}_2$. This particular choice of window length for $\mathbf{A}_1$ tends to separate transients of duration less than approximately 0.3 seconds from the sustained oscillatory waveforms of longer duration. The window length for $\mathbf{A}_2$ is chosen in accordance with the mean duration, 1.25 seconds, of the sleep spindles [36]. Also, the window lengths of 0.32 and 1.28 seconds ensure that the DFT lengths used are powers of 2 at a sampling rate of 100 Hz and 200 Hz.

Note that the dual-BPD algorithm requires the specification of the parameters λ_1, λ_2. For the examples in this section and the experimental study in Section V, we use $\lambda_1 = \lambda_2 = 0.06 \cdot \mathbf{y}_{\text{rms}}$, where the RMS value of $\mathbf{y}$ is defined as (2).

For the raw and unprocessed EEG, it can be seen in Fig. 3, the Wendt algorithm [36] detects two spindles - one starting at 26.2 seconds and the other at 27.6 seconds. However, the experts have classified only one spindle, starting at 26.2 seconds. Thus the Wendt algorithm detects a false positive. On the other hand, when the Wendt algorithm is applied to the dual-BPD processed EEG data, it does not produce this false positive.

To further explain, it can be seen in Fig. 4 that the bandpass filter used by Wendt [36] is excited by the non-oscillatory transients present in the EEG. The dual-BPD algorithm, however, separates the transients from the sustained oscillations. The component $\mathbf{s}_1$ contains most of the transients. Thus, when the dual-BPD processed EEG, $\mathbf{y} - \mathbf{s}_1$, is used for spindle detection, the spindle activity is much more prominent, with respect to the baseline, in the bandpass filtered output.

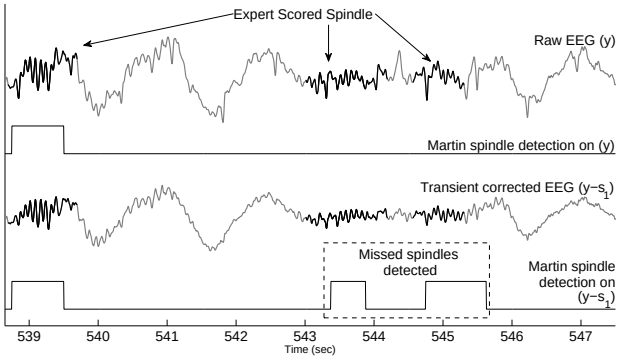

Fig. 5. Spindles originally missed by the Martin algorithm, and their detection on using the dual-BPD processed EEG instead of the raw EEG.

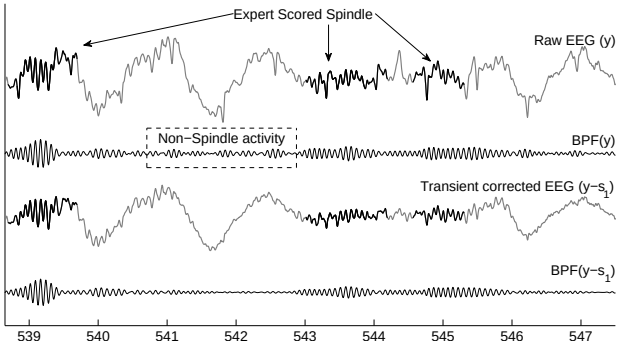

Fig. 6. The input EEG, raw and processed, filtered with the bandpass filter (BPF) used by the Martin algorithm.

As an another example, we consider the Martin algorithm in [20] for sleep spindle detection. Visible in Fig. 5, the experts have annotated 3 sleep spindles starting at 538.8, 543, and 544.6 seconds. However, the Martin algorithm [20] detects only the first spindle. Running the detection on the dual-BPD processed EEG, the Martin algorithm detects the spindles starting at 543 and 544.6 seconds as well.

Once again, it can be seen in Fig. 6 that the bandpass filter used by Martin [20] is excited by the non-oscillatory transients. However, due to the suppression of these transients in $\mathbf{y} - \mathbf{s}_1$, the spindle activity is enhanced, with respect to the baseline, in the filtered output.

V. Experimental Evaluation

To study the performance of the dual-BPD EEG processor for sleep spindle detection, we implement it on the readily available EEG database[1] in [9]. It provides 30 minute excerpts of raw EEG data with annotations for sleep spindles. We apply existing sleep spindle detection algorithms to both raw EEG and EEG processed using dual-BPD.

A. Database

According to [9], the EEG was acquired in a sleep laboratory of a Belgium hospital using a digital 32-channel polygraph (Brain-

[1]University of MONS - TCTS Laboratory (S. Devuyst, T. Dutoit) and Universit Libre de Bruxelles - CHU de Charleroi Sleep Laboratory (M. Kerkhofs) available at http://www.tcts.fpms.ac.be/~devuyst/Databases/DatabaseSpindles/

netTM System of MEDATEC, Brussels, Belgium). The patients from whom the data was obtained, possessed different pathologies (dysomnia,restless legs syndrome, insomnia, apnoea/hypopnoea syndrome) [9]. Three EEG channels (CZ-A1 or C3-A1, FP1-A1, and O1-A1) were recorded in addition to two EOG channels and one submental EMG channel. A segment of 30 minutes of the central EEG channel was extracted from each whole-night recording for sleep spindle scoring. These excerpts were given to two experts who independently scored spindles [9]. The mean age of the 8 patients (male and female) was 46 with standard deviation of 7.45 years.

B. Existing Detection Algorithms

A recent paper [35], studied the performance of 6 widely used sleep spindle detectors. Except for the algorithm in [12][2], we implemented the remaining 5 detectors on the sleep spindle database. We implemented the algorithms with the aid of the software provided in [35], with and without the proposed dual-BPD processor. Below, we detail the detectors and the parameters, changed and unchanged in this paper.

Bódizs et al. [4] - The algorithm detects spindles by bandpass filtering the EEG and calculating Hanning-corrected moving average when a constant threshold is exceeded. It derives spindle frequency boundaries and amplitude criteria, for slow and fast spindles, using the all night average spectrum during stage 2, 3, 4 of sleep. We changed the minimum spindle duration to 0.5 seconds from 0.3 seconds. The boundary frequencies were kept unchanged at 9 Hz and 16 Hz.

Mölle et al. [14] - Spindles are detected by bandpass filtering the EEG, calculating RMS value of the signal in sliding windows and applying a constant threshold. We modified the duration of the spindles to be from 0.5 seconds - 3 seconds as per the manual [32], since the same manual was used by the experts who scored the sleep spindles visually. The frequencies used for the pass-band and stop-band were unchanged.

Martin et al. [20] - The algorithm uses the same procedure as in [14] for sleep spindle detection. The primary difference between the two algorithms is that the Martin algorithm uses a time resolution of 25ms for the windows with no overlap, whereas the Mölle algorithm uses a time resolution of 50ms and 50% overlap. We kept all parameters the same as in [20], except for the spindle duration which was changed to 0.5 seconds - 3 seconds.

Wamsley et al. [34] - Sleep spindles are detected by applying the continuous wavelet transform, using complex Morlet wavelet with center frequency 13.5 Hz and calculating the moving average in sliding windows. We changed the minimum duration of the spindles to 0.5 seconds from 0.3 seconds.

Wendt et al. [36] - The spindle detection algorithm uses both the C3-A1 and the O1-A1 channel of the EEG. It detects spindles by bandpass filtering the EEG and using a time-varying threshold with a given offset. We changed the duration of the spindles to 0.5 seconds - 3 seconds.

C. Statistical Measures of Performance

Using spindle detection by experts as the gold standard, we evaluate the performance of a sleep spindle detector using the by-sample analysis method. In the by-sample analysis, a unit is a sample point of the EEG [35]. A sample point is recorded as a sleep spindle if it was scored as such by both the experts [9].

[2]The detector required the availability of a stage-file which was not provided by the database [9]. The hypnogram provided consisted of 5 sec epochs instead of 30 sec epochs as required by the algorithm.

The sleep spindle detection algorithms output a binary vector, where 1 indicates a spindle and 0 otherwise. Using this binary vector, a 2×2 contingency table can be created to calculate the values of true positive (TP), false positive (FP), true negative (TN) and false negative (FN) for the detectors. These values are used to further calculate the recall (RE) and precision (PR) of the detectors. For the rigorous evaluation of the detectors, with and without the proposed EEG processor, we will use the F_1 score and the Matthews Correlation Coefficient (MCC). Both the scores range from 0 to 1, with 1 denoting the perfect detector.

$$\mathrm{RE} = \frac{\mathrm{TP}}{\mathrm{TP} + \mathrm{FN}} \tag{12a}$$

$$\mathrm{PR} = \frac{\mathrm{TP}}{\mathrm{TP} + \mathrm{FP}} \tag{12b}$$

$$\mathrm{F}_1 = 2 \times \frac{\mathrm{RE} \times \mathrm{PR}}{\mathrm{RE} + \mathrm{PR}} \tag{12c}$$

$$\mathrm{MCC} = \frac{\mathrm{TP} \times \mathrm{TN} - \mathrm{FP} \times \mathrm{FN}}{\sqrt{(\mathrm{TP} + \mathrm{FN})(\mathrm{TP} + \mathrm{FP})(\mathrm{TN} + \mathrm{FP})(\mathrm{TN} + \mathrm{FN})}} \tag{12d}$$

The MCC provides a balanced evaluation of the detector [3]. Moreover, since the spindles are rare events the TN values will be high. Hence, the MCC and F_1 score provide better evaluation of the detector as compared to only sensitivity and specificity values.

D. Results

The dual-BPD processed EEG (C3-A1 channel) was used for sleep spindle detection. We used the same parameters for the dual-BPD algorithm and the window lengths for the transforms $\mathbf{A}_1, \mathbf{A}_2$ as in Section IV.

The F_1 score and further statistics for each of the detectors and their corresponding improvement with the proposed dual-BPD processor were recorded and are listed in the appendix. Also available are the TP, FP, TN, and FN values from which further evaluation can be carried out by the reader. The dual-BPD and the detection algorithms were run on a 2.50 Ghz Intel core i5 machine. The dual-BPD algorithm takes 40 seconds to run 60 iterations on an input EEG signal of 30 minutes with a sampling frequency of 200 Hz.

E. Discussion

For the Martin algorithm [20], the TP values were increased by as much as 23% due to which the RE values increased on an average by 7.8% over the 8 patients. The Wendt algorithm [36] saw a reduction in FP values by as much as 59% thereby increasing the PR values by 14% on an average.

When detecting spindles with the dual-BPD processed EEG, the F_1 scores of the detectors, on an average, improved by 13.3%. The MCC score of these detectors was also improved by 13.9%. The improvement in the F_1 score ranged from 2% to as much as 38% with a similar range of improvement in the MCC score.

The suppression of the non-oscillatory transient waves in the EEG, using dual-BPD, leads to fewer FP values. As a result, the performance of the spindle detection algorithms in Section V-B is improved when they are applied on the dual-BPD processed EEG as compared to the raw EEG.

Indirectly, the experimental study assesses the performance of the 5 spindle detectors on a database different than the one used for their design. Among the detectors, the Wamsley algorithm [34] performed the worst as compared to its performance in [35] where it surpassed the other detectors. It was hardly able to detect spindles in all but one of the 30 min excerpts. The Martin algorithm [20] achieved the highest F_1 score of 0.64 with the proposed EEG processor and 0.60 without it.

It is worth noting that the algorithms in Section V-B were tested on healthy subjects in contrast to the database [9] on which we tested them.

VI. Conclusion

This paper proposes to improve the performance of existing sleep spindle detection algorithms by pre-processing the raw EEG using dual-BPD. The non-linear dual-BPD method separates the non-oscillatory transient and the sustained rhythmic oscillations components. The non-oscillatory transient component is not used for spindle detection. When the rhythmic oscillations component is filtered, the spindle activity is much more prominent with respect to the baseline. This leads to an increase in the true positive values of the sleep spindle detectors and a decrease in the false positive values of the detectors. This increases the F_1 score of the spindle detection algorithms. The dual-BPD processor was able to increase the F_1 score by 13.3% on an average, with a similar range of improvement in the Matthews Correlation Coefficient of the detectors.

The results suggest that the proposed dual-BPD processor for EEG signals may be used to enhance sleep spindle detection. Since sleep spindle detection is an important component of sleep scoring, it would be desirable to further validate the results on a wider database including full nights of sleep EEG in both, normal and patient populations.

References

[1] N. Acir and C. Güzeli, "Automatic recognition of sleep spindles in EEG via radial basis support vector machine based on a modified feature selection algorithm," *Neural Comput. Appl.*, vol. 14, no. 1, pp. 56–65, Jan. 2005.

[2] M. Afonso, J. M. Bioucas-Dias, and M. A. T. Figueiredo, "Fast image recovery using variable splitting and constrained optimization." *IEEE Trans. Image Process.*, vol. 19, pp. 2345–2356, 2010.

[3] P. Baldi, S. Brunak, Y. Chauvin, C. A. Andersen, and H. Nielsen, "Assessing the accuracy of prediction algorithms for classification: an overview." *Bioinformatics*, vol. 16, pp. 412–424, 2000.

[4] R. Bódizs, J. Körmendi, P. Rigó, and A. S. Lázár, "The individual adjustment method of sleep spindle analysis: methodological improvements and roots in the fingerprint paradigm." *J. Neurosci. Methods*, vol. 178, no. 1, pp. 205–13, Mar. 2009.

[5] S. Chen, D. L. Donoho, and M. A. Saunders, "Atomic decomposition by basis pursuit," *SIAM J. Sci. Comput.*, vol. 43, no. 1, pp. 129–159, 1998.

[6] L. Cohen, "Time-frequency distributions - a review," pp. 941–981, 1989.

[7] J. Costa, M. Ortigueira, A. Batista, and L. Paiva, "An Automatic Sleep Spindle detector based on WT, STFT and WMSD," *World Acad. Sci. Eng. Technol.*, pp. 1833–1836, 2012.

[8] S. Devuyst, T. Dutoit, J. Didier, F. Meers, E. Stanus *et al.*, "Automatic sleep spindle detection in patients with sleep disorders," *Proc. IEEE Int. Conf. Eng. Med. Biol. (EMBC)*, pp. 3883–3886, Aug. 2006.

[9] S. Devuyst, T. Dutoit, P. Stenuit, and M. Kerkhofs, "Automatic sleep spindles detection - overview and development of a standard proposal assessment method." *Proc. IEEE Int. Conf. Eng. Med. Biol. (EMBC)*, pp. 1713–1716, Aug. 2011.

[10] D. L. Donoho, "De-noising by soft-thresholding," *IEEE Trans. Inf. Theory*, vol. 41, pp. 613–627, 1995.

[11] P. J. Durka and K. J. Blinowska, "Matching pursuit parametrization of sleep spindles," *Eng. Med. Biol.*, vol. 3, pp. 1011–1012, Oct. 1996.

[12] F. Ferrarelli, R. Huber, M. J. Peterson, M. Massimini, M. Murphy *et al.*, "Reduced sleep spindle activity in schizophrenia patients." *Am. J. Psychiatry*, vol. 164, no. 3, pp. 483–92, Mar. 2007.

[13] S. M. Fogel and C. T. Smith, "The function of the sleep spindle: a physiological index of intelligence and a mechanism for sleep-dependent memory consolidation." *Neurosci. Biobehav. Rev.*, vol. 35, no. 5, pp. 1154–65, Apr. 2011.

[14] S. Gais, M. Mölle, K. Helms, and J. Born, "Learning-dependent increases in sleep spindle density." *J. Neurosci.*, vol. 22, no. 15, pp. 6830–4, Aug. 2002.

[15] D. Gorur, U. Halici, and H. Aydin, "Sleep spindles detection using short time Fourier transform and neural networks," *Int. Jt. Conf. Neural Networks (IJCNN)*, pp. 1631–1636, 2002.

[16] E. Huupponen, W. De Clercq, G. Gómez-Herrero, A. Saastamoinen, K. Egiazarian *et al.*, "Determination of dominant simulated spindle frequency with different methods." *J. Neurosci. Methods*, vol. 156, no. 1-2, pp. 275–83, Sep. 2006.

[17] E. Huupponen, G. Gómez-Herrero, A. Saastamoinen, A. Värri, J. Hasan *et al.*, "Development and comparison of four sleep spindle detection methods." *Artif. Intell. Med.*, vol. 40, no. 3, pp. 157–70, Jul. 2007.

[18] E. Limoges, L. Mottron, C. Bolduc, C. Berthiaume, and R. Godbout, "Atypical sleep architecture and the autism phenotype." *Brain*, vol. 128, no. Pt 5, pp. 1049–61, May 2005.

[19] S. Mallat and Z. Zhang, "Matching pursuits with time-frequency dictionaries," *Signal Process. IEEE Trans.*, 1993.

[20] N. Martin, M. Lafortune, J. Godbout, M. Barakat, R. Robillard *et al.*, "Topography of age-related changes in sleep spindles." *Neurobiol. Aging*, vol. 34, no. 2, pp. 468–76, Feb. 2013.

[21] S. Motamedi-Fakhr, M. Moshrefi-Torbati, M. Hill, C. M. Hill, and P. R. White, "Signal processing techniques applied to human sleep EEG signals: A review," *Biomed. Signal Process. Control*, vol. 10, pp. 21–33, Mar. 2014.

[22] R. G. Norman, J. A. Walsleben, R. Zozula, and D. M. Rapoport, "A likelihood based computer approach to conventional scoring of sleep," *Proc. IEEE Int. Conf. Eng. Med. Biol. (EMBC)*, pp. 2645–2646, 1992.

[23] D. Petit, J. F. Gagnon, M. L. Fantini, L. Ferini-Strambi, and J. Montplaisir, "Sleep and quantitative EEG in neurodegenerative disorders," pp. 487–496, 2004.

[24] L. B. Ray, S. M. Fogel, C. T. Smith, and K. R. Peters, "Validating an automated sleep spindle detection algorithm using an individualized approach." *J. Sleep Res.*, vol. 19, no. 2, pp. 374–8, Jun. 2010.

[25] A. Rechtshaffen and A. Kales, *A manual of standardized terminology, techniques and scoring system for sleep stages of human subjects*, 1968.

[26] P. Schimicek, J. Zeitlhofer, P. Anderer, and B. Saletu, "Automatic sleep-spindle detection procedure: aspects of reliability and validity." *Clin. Electroencephalogr.*, vol. 25, pp. 26–29, 1994.

[27] S. V. Schönwald, E. L. de Santa-Helena, R. Rossatto, M. L. F. Chaves, and G. J. L. Gerhardt, "Benchmarking matching pursuit to find sleep spindles." *J. Neurosci. Methods*, vol. 156, no. 1-2, pp. 314–21, Sep. 2006.

[28] I. W. Selesnick, "Short-time Fourier transform and its inverse," *http://cnx.org/content/m32294/*, 2009.

[29] I. W. Selesnick, "Resonance-based signal decomposition: A new sparsity-enabled signal analysis method," *Signal Processing*, vol. 91, pp. 2793–2809, 2011.

[30] I. W. Selesnick, "L1-norm penalized least squares with SALSA," *http://cnx.org/content/m48933/*, 2014.

[31] I. W. Selesnick, K. Y. Li, S. U. Pillai, and B. Himed, "Doppler-streak attenuation via oscillatory-plus-transient decomposition of IQ data," *IET Int. Conf. Radar Syst.*, pp. 24–24, 2012.

[32] M. H. Silber, S. Ancoli-Israel, M. H. Bonnet, S. Chokroverty, M. M. Grigg-Damberger *et al.*, "The visual scoring of sleep in adults." *J. Clin. Sleep Med.*, vol. 3, no. 2, pp. 121–31, Mar. 2007.

[33] J.-L. Starck, M. Elad, and D. L. Donoho, "Image decomposition via the combination of sparse representations and a variational approach." *IEEE Trans. Image Process.*, vol. 14, no. 10, pp. 1570–82, Oct. 2005.

[34] E. Wamsley, M. Tucker, and A. Shinn, "Reduced sleep spindles and spindle coherence in schizophrenia: mechanisms of impaired memory consolidation?" *Biol Psychiatry*, vol. 71, no. 2, pp. 154–161, 2012.

[35] S. C. Warby, S. L. Wendt, P. Welinder, E. G. S. Munk, O. Carrillo *et al.*, "Sleep-spindle detection: crowdsourcing and evaluating performance of experts, non-experts and automated methods." *Nat. Methods*, vol. 11, no. 4, pp. 385–92, Apr. 2014.

[36] S. L. Wendt, J. E. Christensen, J. Kempfner, H. L. Leonthin, P. Jennum *et al.*, "Validation of a novel automatic sleep spindle detector with high performance during sleep in middle aged subjects," *Proc. IEEE Int. Conf. Eng. Med. Biol.*, pp. 4250–4253, Aug. 2012.

[37] J. Zeitlhofer and G. Gruber, "Topographic distribution of sleep spindles in young healthy subjects," *J. Sleep Res.*, vol. 6, no. 3, pp. 149–155, 1997.

[38] J. Zygierewicz, K. J. Blinowska, P. J. Durka, W. Szelenberger, S. Niemcewicz *et al.*, "High resolution study of sleep spindles." *Clin. Neurophysiol.*, vol. 110, pp. 2136–2147, 1999.

APPENDIX
Performance and Statistics

Excerpt1	Wendt	Processed Wendt	Martin	Processed Martin	Wamsley	Processed Wamsley	Bodizs	Processed Bodizs	Molle	Processed Moelle
TP	8357	7605	4121	4519	2374	2657	9550	10151	4991	6164
TN	156774	161922	164771	165494	166242	166314	137540	135673	164911	164734
FP	9751	4603	1754	1031	283	211	28985	30852	1614	1791
FN	5118	5870	9354	8956	11101	10818	3925	3324	8484	7311
Recall	0.620	0.564	0.306	0.335	0.176	0.197	0.709	0.753	0.370	0.457
Precision	0.462	0.623	0.701	0.814	0.893	0.926	0.248	0.248	0.756	0.775
F1 Score	**0.529**	**0.592**	**0.426**	**0.475**	**0.294**	**0.325**	**0.367**	**0.373**	**0.497**	**0.575**
SPC	0.941	0.972	0.989	0.994	0.998	0.999	0.826	0.815	0.990	0.989
NPV	0.968	0.965	0.946	0.949	0.937	0.939	0.972	0.976	0.951	0.958
Accuracy	0.917	0.942	0.938	0.945	0.937	0.939	0.817	0.810	0.944	0.949
Kappa	**0.485**	**0.561**	**0.399**	**0.451**	**0.276**	**0.307**	**0.288**	**0.293**	**0.471**	**0.550**
MCC	**0.491**	**0.562**	**0.437**	**0.501**	**0.381**	**0.412**	**0.343**	**0.356**	**0.505**	**0.572**

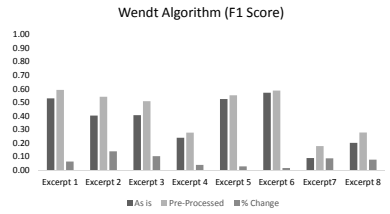

Excerpt3	Wendt	Processed Wendt	Martin	Processed Martin	Wamsley	Processed Wamsley	Bodizs	Processed Bodizs	Molle	Processed Moelle
TP	1005	1013	680	973	12	40			0	0
TN	86050	87031	87234	87313	86741	86146			87717	87717
FP	1667	686	483	404	976	1571			0	0
FN	1278	1270	1603	1310	2271	2243			2283	2283
Recall	0.440	0.444	0.298	0.426	0.005	0.018			0.000	0.000
Precision	0.376	0.596	0.585	0.707	0.012	0.025	Not recorded		0.000	0.000
F1 Score	**0.406**	**0.509**	**0.395**	**0.532**	**0.007**	**0.021**			**0.000**	**0.000**
SPC	0.981	0.992	0.994	0.995	0.989	0.982			1.000	1.000
NPV	0.985	0.986	0.982	0.985	0.974	0.975			0.975	0.975
Accuracy	0.967	0.978	0.977	0.981	0.964	0.958			0.975	0.975
Kappa	**0.389**	**0.498**	**0.384**	**0.523**	**-0.008**	**0.000**			**0.000**	**0.000**
MCC	**0.390**	**0.504**	**0.407**	**0.540**	**-0.009**	**0.000**			**0.000**	**0.000**

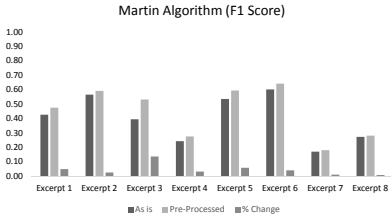

Excerpt5	Wendt	Processed Wendt	Martin	Processed Martin	Wamsley	Processed Wamsley	Bodizs	Processed Bodizs	Molle	Processed Moelle
TP	10265	10735	9672	10925	0	150	14779	15061	0	0
TN	331120	331841	333514	334112	337779	337630	295704	297552	340039	340039
FP	8919	8198	6525	5927	2260	2409	44335	42487	0	0
FN	9696	9226	10289	9036	19961	19811	5182	4900	19961	19961
Recall	0.514	0.538	0.485	0.547	0.000	0.008	0.740	0.755	0.000	0.000
Precision	0.535	0.567	0.597	0.648	0.000	0.059	0.250	0.262	0.000	0.000
F1 Score	**0.524**	**0.552**	**0.535**	**0.594**	**0.000**	**0.013**	**0.374**	**0.389**	**0.000**	**0.000**
SPC	0.974	0.976	0.981	0.983	0.993	0.993	0.870	0.875	1.000	1.000
NPV	0.972	0.973	0.970	0.974	0.944	0.945	0.983	0.984	0.945	0.945
Accuracy	0.948	0.952	0.953	0.958	0.938	0.938	0.862	0.868	0.945	0.945
Kappa	**0.497**	**0.526**	**0.511**	**0.572**	**-0.011**	**0.001**	**0.317**	**0.334**	**0.000**	**0.000**
MCC	**0.497**	**0.527**	**0.514**	**0.574**	**-0.019**	**0.001**	**0.377**	**0.393**	**0.000**	**0.000**

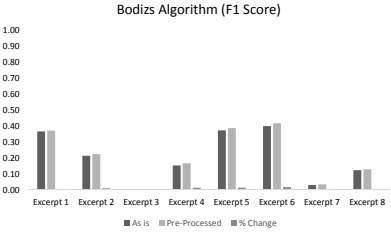

Excerpt7	Wendt	Processed Wendt	Martin	Processed Martin	Wamsley	Processed Wamsley	Bodizs	Processed Bodizs	Molle	Processed Moelle
TP	1340	1358	1752	2017	0.000	0.000	1339	1648	0	0
TN	331445	346026	341105	339655	356199	355653	272664	265978	357044	357044
FP	25599	11018	15939	17389	845	1391	84380	91066	0	0
FN	1616	1598	1204	939	2956	2956	1617	1308	2956	2956
Recall	0.453	0.459	0.593	0.682	0.000	0.000	0.453	0.558	0.000	0.000
Precision	0.050	0.110	0.099	0.104	0.000	0.000	0.016	0.018	0.000	0.000
F1 Score	**0.090**	**0.177**	**0.170**	**0.180**	**0.000**	**0.000**	**0.030**	**0.034**	**0.000**	**0.000**
SPC	0.928	0.969	0.955	0.951	0.998	0.996	0.764	0.745	1.000	1.000
NPV	0.995	0.995	0.996	0.997	0.992	0.992	0.994	0.995	0.992	0.992
Accuracy	0.924	0.965	0.952	0.949	0.989	0.988	0.761	0.743	0.992	0.992
Kappa	**0.076**	**0.166**	**0.158**	**0.169**	**-0.004**	**-0.005**	**0.015**	**0.019**	**0.000**	**0.000**
MCC	**0.131**	**0.212**	**0.229**	**0.253**	**-0.004**	**-0.006**	**0.046**	**0.062**	**0.000**	**0.000**

Excerpt2	Wendt	Processed Wendt	Martin	Processed Martin	Wamsley	Processed Wamsley	Bodizs	Processed Bodizs	Molle	Processed Moelle
TP	9881	6169	7954	9394	0	0	11045	12005	7006	10516
TN	320771	343386	339807	337600	344818	344917	268002	265126	340517	326124
FP	24754	2139	5718	7925	707	608	77523	80399	5008	19401
FN	4594	8306	6521	5081	14475	14475	3430	2470	7469	3959
Recall	0.683	0.426	0.549	0.649	0.000	0.000	0.763	0.829	0.484	0.726
Precision	0.285	0.743	0.582	0.542	0.000	0.000	0.125	0.130	0.583	0.352
F1 Score	**0.402**	**0.542**	**0.565**	**0.591**	**0.000**	**0.000**	**0.214**	**0.225**	**0.529**	**0.474**
SPC	0.928	0.994	0.983	0.977	0.998	0.998	0.776	0.767	0.986	0.944
NPV	0.986	0.976	0.981	0.985	0.960	0.960	0.987	0.991	0.979	0.988
Accuracy	0.918	0.971	0.966	0.964	0.958	0.958	0.775	0.770	0.965	0.935
Kappa	**0.366**	**0.528**	**0.548**	**0.572**	**-0.004**	**-0.003**	**0.156**	**0.167**	**0.511**	**0.444**
MCC	**0.407**	**0.549**	**0.548**	**0.575**	**-0.009**	**-0.008**	**0.246**	**0.268**	**0.514**	**0.477**

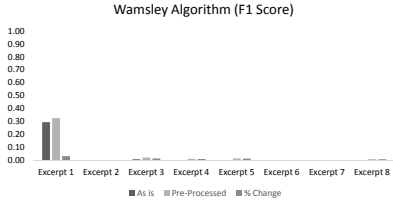

Excerpt4	Wendt	Processed Wendt	Martin	Processed Martin	Wamsley	Processed Wamsley	Bodizs	Processed Bodizs	Molle	Processed Moelle
TP	3710	4181	3458	4254	0	112	7301	7783	0	0
TN	332639	334003	334975	333344	338439	337841	272161	274664	346380	346380
FP	13741	12377	11405	13036	7941	8539	74219	71716	0	0
FN	9910	9439	10162	9366	13620	13508	6319	5837	13620	13620
Recall	0.272	0.307	0.254	0.312	0.000	0.008	0.536	0.571	0.000	0.000
Precision	0.213	0.253	0.233	0.246	0.000	0.013	0.090	0.098	0.000	0.000
F1 Score	**0.239**	**0.277**	**0.243**	**0.275**	**0.000**	**0.010**	**0.153**	**0.167**	**0.000**	**0.000**
SPC	0.960	0.964	0.967	0.962	0.977	0.975	0.786	0.793	1.000	1.000
NPV	0.971	0.973	0.971	0.973	0.961	0.962	0.977	0.979	0.962	0.962
Accuracy	0.934	0.939	0.940	0.938	0.940	0.939	0.776	0.785	0.962	0.962
Kappa	**0.205**	**0.246**	**0.212**	**0.243**	**-0.029**	**-0.020**	**0.095**	**0.110**	**0.000**	**0.000**
MCC	**0.207**	**0.247**	**0.212**	**0.245**	**-0.030**	**-0.020**	**0.147**	**0.168**	**0.000**	**0.000**

Excerpt6	Wendt	Processed Wendt	Martin	Processed Martin	Wamsley	Processed Wamsley	Bodizs	Processed Bodizs	Molle	Processed Moelle
TP	12810	13317	11724	13001	0	0	17988	17182	11928	12385
TN	327975	327928	332715	332462	336704	336333	288379	295169	331078	330729
FP	9588	9635	4848	5101	859	1230	49184	42394	6485	6834
FN	9627	9120	10713	9436	22437	22437	4449	5255	10509	10052
Recall	0.571	0.594	0.523	0.579	0.000	0.000	0.802	0.766	0.532	0.552
Precision	0.572	0.580	0.707	0.718	0.000	0.000	0.268	0.288	0.648	0.644
F1 Score	**0.571**	**0.587**	**0.601**	**0.641**	**0.000**	**0.000**	**0.401**	**0.419**	**0.584**	**0.595**
SPC	0.972	0.971	0.986	0.985	0.997	0.996	0.854	0.874	0.981	0.980
NPV	0.971	0.973	0.969	0.972	0.938	0.937	0.985	0.983	0.969	0.971
Accuracy	0.947	0.948	0.957	0.960	0.935	0.934	0.851	0.868	0.953	0.953
Kappa	**0.543**	**0.559**	**0.579**	**0.620**	**-0.005**	**-0.007**	**0.340**	**0.361**	**0.559**	**0.570**
MCC	**0.543**	**0.559**	**0.586**	**0.624**	**-0.013**	**-0.015**	**0.407**	**0.416**	**0.562**	**0.572**

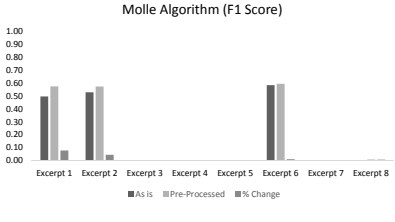

Excerpt8	Wendt	Processed Wendt	Martin	Processed Martin	Wamsley	Processed Wamsley	Bodizs	Processed Bodizs	Molle	Processed Moelle
TP	4840	3685	3008	3192	0	44	5207	5593	0	**0**
TN	316707	337180	340902	340431	174090	171641	281643	279229	175797	175797
FP	34935	14462	10740	11211	1707	4156	69999	72413	0	0
FN	3518	4673	5350	5166	4203	4159	3151	2765	4203	4203
Recall	0.579	0.441	0.360	0.382	0.000	0.010	0.623	0.669	0.000	0.000
Precision	0.122	0.203	0.219	0.222	0.000	0.010	0.069	0.072	0.000	0.000
F1 Score	**0.201**	**0.278**	**0.272**	**0.280**	**0.000**	**0.010**	**0.125**	**0.130**	**0.000**	**0.000**
SPC	0.901	0.959	0.969	0.968	0.990	0.976	0.801	0.794	1.000	1.000
NPV	0.989	0.986	0.985	0.985	0.976	0.976	0.989	0.990	0.977	0.977
Accuracy	0.893	0.947	0.955	0.955	0.967	0.954	0.797	0.791	0.977	0.977
Kappa	**0.169**	**0.254**	**0.250**	**0.259**	**-0.014**	**-0.013**	**0.086**	**0.091**	**0.000**	**0.000**
MCC	**0.230**	**0.275**	**0.259**	**0.269**	**-0.015**	**-0.013**	**0.157**	**0.169**	**0.000**	**0.000**